Eur. Phys. J. Plus (2019) **134**: 530
DOI 10.1140/epjp/i2019-12906-5

THE EUROPEAN PHYSICAL JOURNAL PLUS

Regular Article

Two-dimensional induced grating in Rydberg atoms via microwave field

Tayebeh Naseri[a]

Department of Physics, Razi University, Kermanshah, Iran

Received: 23 May 2019 / Revised: 17 July 2019
Published online: 23 October 2019

Abstract. A novel two-dimensional phase and amplitude electromagnetically induced grating is proposed. This model improves the sensitivity of electromagnetically induced grating to the microwave field. The system experiences electromagnetically induced transparency (EIT) via interacting dark resonances. When two-dimensional standing control fields are applied to a Rydberg five-level EIT system, two sub-EIT systems appear and the central peak in the EIT window is splitted. Frequency splitting of two central absorption peaks is proportional to the microwave field strength. The simulations show that the efficiency of higher orders of two-dimensional EIG could be enhanced compared to a common four-level single-dark-state system without microwave field. Therefore, one can take advantage of the phase modulation to control the probe light dispersing into the required high orders. This proposed model is appropriate to be utilized as an all-optical switch and router in optical networking and communication based on microwave field.

1 Introduction

Quantum coherence and interference have substantial functions in modifying and controlling the optical response of a medium and have been attracted extensively attention in recent years. Electromagnetically induced transparency (EIT) based on quantum coherence and interference, refers to the medium that becomes transparent to a probe laser field just by means of another strong coupling field. EIT has been significantly investigated in recent years for its novel potential applications such as giant Kerr nonlinearity [1], slow light [2], optical bistability and multistability [3], four-wave mixing [4]. Electromagnetically induced grating (EIG) as a consequence of EIT, can be observed via applying a strong standing control field in the EIT medium. By means of the standing field, the probe field experiences periodic modulation in space. Consequently, the Fraunhofer diffraction of the probe field is created. EIG has been investigated in different media such as hot and cold atoms theoretically and experimentally [5–7].

EIG has attracted growing attention due to its potential applications, for example, electromagnetically induced Talbot effect, surface solitons, polarization-dependent multiple beam splitting in the Raman-Nath limit [8].

To improve and modify the higher-order diffraction efficiency in an EIG medium, so many models have been proposed and explored in multi-level atomic systems. For instance, EIG in the coherent population trapping (CPT) condition in a four-level microwave driven N-type atomic system has studied in which a novel nonlinear optical storage was obtained via linear absorption vanishing and giant Kerr nonlinearity during light propagation [9]. Moreover, efficient electromagnetically induced phase grating by spontaneous generated coherence (SGC) was studied [10]. EIG in an asymmetric semiconductor quantum well (SQW) structure via Fano interference has been proposed [11]. Also, gain-phase grating (GPG) based on the spatial modulation of active Raman gain has theoretically studied [12] and another novel EIG scheme in a monolayer graphene nanostructure under Raman excitation has also investigated [13].

The huge electric-dipole moments, large extensions of the electronic wave functions, long radiative lifetimes and extreme sensitivity to external electric fields of Rydberg atoms, make them very interesting to investigate quantum optics phenomena experimentally to overcome the main drawback of practical implementation of microscopic quantum objects. Newly, EIG in an ensemble of strongly interacting Rydberg atoms has been proposed [14,15]. Since the size of Rydberg atoms is huge, the geometric cross section of the medium is tunable and, consequently, their response and, sensitivity to the external electromagnetic fields is enhanced [16]. Recently, multi-level Rydberg atoms have been used for microwave field sensing [17,18].

[a] e-mail: tayebe.naseri@gmail.com

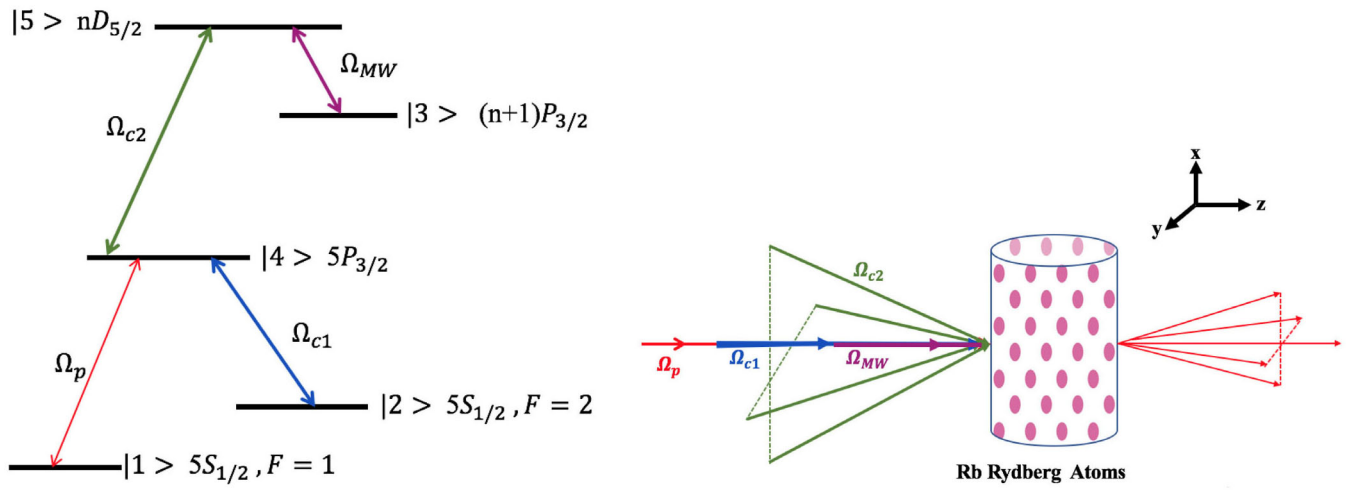

(a) (b)

Fig. 1. (a) The schematic diagram of the five-level system for the 87Rb Rydberg atom. (b) The schematic diagram of the microwave and coupling fields and probe field propagating through the cold atomic medium.

All of the aforementioned schemes were concentrated on the one-dimensional EIG (1D EIG) via quantum coherence and interference in multi-level different media. Two-dimensional electromagnetically induced cross-grating in two-level [19], three-level [20], four-level tripod-type [21] and N-type atomic systems [22] have been offered lately.

To our knowledge, the relevant topic of exploring controllable 2D EIG in Rydberg atoms by means microwave field has received little attention. In this paper, we propose an efficient scheme for two-dimensional EIG with Rydberg atoms via microwave field. When the microwave field drives an assistant transition of a common four-level single-dark-state system, the system becomes a five-level double-dark-state one. By exploring the impact of a MW field on the linear susceptibility and applying standing field coupling, the two-dimensional EIG is studied. In comparison with the two-dimensional amplitude electromagnetically induced grating based on electromagnetically induced transparency, the two-dimensional phase grating has much higher diffraction intensities in the first order of the high-order directions. Therefore, it is appropriate to be utilized as all-optical switches and routers as a microwave field sensing in optical networking and communication.

This paper is prepared as follows: In sect. 2 theoretical model and the governing equations are presented. In sect. 3, by using microwave and two cross standing-wave coupling fields, the 2D spatial modulation of the absorption and dispersion is studied to obtain Fraunhofer diffraction patterns. The conclusion is offered in sect. 4.

2 Theoretical model and methods

Let us consider a five-level double-dark resonance state system for Rydberg rubidium 87 in the present study as shown in fig. 1. Various experimental implementations of the above scheme could be used. For example in cold Rydberg rubidium 87, the two hyperfine ground levels $|1\rangle$ and $|2\rangle$ with $5S_{1/2}$, $F = 1, 2$ can be chosen. $(n+1)P_{3/2}$ to be $|3\rangle$, $5P_{3/2}$ to be $|4\rangle$ and $nD_{5/2}$ to be $|5\rangle$.

A weak probe laser field couples the transition $|1\rangle \leftrightarrow |4\rangle$ with Rabi frequency Ω_p. The transition $|2\rangle \leftrightarrow |4\rangle$ is driven by a laser field with Rabi frequency Ω_{c1}. $|4\rangle \leftrightarrow |5\rangle$ transition is driven by the superposition of two orthogonal standing-wave fields with Rabi frequency $\Omega_{c2} = \Omega[\sin(\pi x/\Lambda_x) + \sin(\pi y/\Lambda_y)]$.

Moreover, a microwave field (MW) couples the transition $|3\rangle \leftrightarrow |5\rangle$ with respective Rabi frequency Ω_M. The detuning parameters Δ_i are given by $\Delta_p = \omega_p - \omega_{41}$, $\Delta_{c1} = \omega_{c1} - \omega_{42}$, $\Delta_{c2} = \omega_{c2} - \omega_{45}$, and $\Delta_M = \omega_M - \omega_{53}$. It should be noticed that the Doppler broadening and the van der Waals (vdW) interaction are not considered in the calculations.

After applying the dipole approximation and the rotating wave approximation (RWA), the Hamiltonian of this multi-level system becomes

$$\begin{aligned} H_I = -\hbar[&(\Delta_p - \Delta_{c1})\,|2\rangle\langle 2| + (\Delta_p + \Delta_{c2} - \Delta_M)\,|3\rangle\langle 3| + \Delta_p\,|4\rangle\langle 4| \\ &+ (\Delta_p + \Delta_{c2})\,|5\rangle\langle 5| + \Omega_p\,|4\rangle\langle 1| + \Omega_{c2}\,|5\rangle\langle 4| + \Omega_{c1}\,|4\rangle\langle 2| + \Omega_M\,|5\rangle\langle 3| + h.c.], \end{aligned} \tag{1}$$

where "$h.c.$" is the Hermitian conjugate of the preceding off-diagonal terms. The master equation then takes the form

$$\dot{\rho} = -\frac{i}{\hbar}[H_I, \rho] + L\rho, \tag{2}$$

in terms of the density-matrix operator ρ. $L\rho$ indicates the decay part of the system. After applying the Hamiltonian of eq. (1) to the master equation, inserting the expressions for the decay rates, and transforming in standard fashion, one obtains:

$$\begin{aligned}
\dot{\rho}_{11} &= \gamma_{41}\rho_{44} - i\Omega_p(\rho_{14} - \rho_{41}) \\
\dot{\rho}_{22} &= \gamma_{42}\rho_{44} - i\Omega_{c1}(\rho_{24} - \rho_{42}) \\
\dot{\rho}_{44} &= -[\gamma_{41} + \gamma_{42}]\rho_{44} + \gamma_{54}\rho_{55} - i\Omega_p(\rho_{41} - \rho_{14}) - i\Omega_{c1}(\rho_{42} - \rho_{24}) - i\Omega_{c2}(\rho_{45} - \rho_{54}) \\
\dot{\rho}_{55} &= -[\gamma_{53} + \gamma_{54}]\rho_{55} - i\Omega_M(\rho_{53} - \rho_{35}) - i\Omega_{c2}(\rho_{54} - \rho_{45}) \\
\dot{\rho}_{21} &= -[\gamma_{21} + i(\Delta_{c1} - \Delta_p)]\rho_{21} - i\Omega_p\rho_{24} + i\Omega_{c1}\rho_{41} \\
\dot{\rho}_{31} &= -[\gamma_{31} - i(\Delta_p + \Delta_{c2} - \Delta_M)]\rho_{31} + i\Omega_p\rho_{34} + i\Omega_M\rho_{51} \\
\dot{\rho}_{41} &= -[\gamma_{41} - i\Delta_p]\rho_{41} - i\Omega_p(\rho_{44} - \rho_{11}) + i\Omega_{c1}\rho_{21} + i\Omega_{c2}\rho_{51} \\
\dot{\rho}_{51} &= -[\gamma_{51} - i(\Delta_p + \Delta_{c2})]\rho_{51} + i\Omega_{c2}\rho_{41} + i\Omega_M\rho_{31} - i\Omega_p\rho_{54} \\
\dot{\rho}_{32} &= -[\gamma_{32} - i(\Delta_{c1} + \Delta_{c1} - \Delta_M)]\rho_{32} - i\Omega_{c1}\rho_{34} + i\Omega_M\rho_{52} \\
\dot{\rho}_{42} &= -[\gamma_{42} - i\Delta_{c1}]\rho_{42} + i\Omega_{c1}(\rho_{22} - \rho_{44}) + i\Omega_p\rho_{12} + i\Omega_{c2}\rho_{52} \\
\dot{\rho}_{52} &= -[\gamma_{52} - i(\Delta_{c1} + \Delta_{c2})]\rho_{52} + i\Omega_M\rho_{32} + i\Omega_{c2}\rho_{42} - i\Omega_{c1}\rho_{54} \\
\dot{\rho}_{34} &= -[\gamma_{43} - i(\Delta_{c2} - \Delta_{c1})]\rho_{34} - i\Omega_p\rho_{31} - i\Omega_{c1}\rho_{32} - i\Omega_{c2}\rho_{35} + i\Omega_M\rho_{54} \\
\dot{\rho}_{54} &= -[\gamma_{54} - i\Delta_{c2}]\rho_{54} + i\Omega_M\rho_{34} + i\Omega_{c2}(\rho_{44} - \rho_{55}) - i\Omega_p\rho_{51} - i\Omega_{c1}\rho_{52},
\end{aligned} \tag{3}$$

where $\gamma_{ij} = (\Gamma_i + \Gamma_j)/2$, $\Gamma_i = \sum_k \Gamma_{ik}$, Γ_{ik} is the spontaneous relaxation rate from the states $|i\rangle$ to $|k\rangle$. The beyond equations follow from the constraints:

$$\rho_{11} + \rho_{22} + \rho_{33} + \rho_{44} + \rho_{55} = 1; \qquad \rho_{ij} = \rho_{ij}^*, \tag{4}$$

since the probe field is much weaker than the other coupling fields. Considering the initial conditions are $\rho_{11}^{(0)} = 1$ and other elements $\rho_{ij}^{(0)} = 0$, the steady state solution can be calculated using the iterative method:

$$\rho_{41}^{(1)} = \frac{i\Omega_p}{\Gamma_4 + \frac{\Omega_{c1}^2}{\Gamma_2} + \frac{\Omega_{c2}^2}{\Gamma_5 + \frac{\Omega_M^2}{\Gamma_3}}}, \tag{5}$$

$$\begin{aligned}
\Gamma_2 &= \gamma_{21} + i(\Delta_{c1} - \Delta_p) \\
\Gamma_3 &= \gamma_{31} - i(\Delta_p + \Delta_{c2} - \Delta_M) \\
\Gamma_4 &= \gamma_{41} - i\Delta_p \\
\Gamma_5 &= \gamma_{51} - i(\Delta_p + \Delta_{c2}).
\end{aligned} \tag{6}$$

Therefore, the linear susceptibility of the probe field can be defined as

$$\chi_{41} = \frac{2N_0|\mu_{41}|^2}{\epsilon_0\hbar\Omega_p}\rho_{41}^{(1)}, \tag{7}$$

where N_0 is the atom number density and ϵ_0 is the permitivity in the free space. As depicted in fig. 1(b), the probe field propagates along the z-direction through a cold atomic sample of length L.

Under the slowly varying amplitude approximation and in the steady state, Maxwell's equation describes the probe field propagation [23],

$$\frac{\partial\Omega_p}{\partial z} = i\chi_{41}\Omega_p. \tag{8}$$

By solving the above equation, the transmission function of the probe field through the atomic medium at $z = L$ can be obtained

$$T(x, y) = e^{i\chi_{41}L}. \tag{9}$$

Consequently, the phase of the transmission function is calculated

$$\phi(x, y) = Re[\chi_{41}]L. \tag{10}$$

For a plane probe wave, the intensity distribution in the far field for Fraunhofer diffraction is given

$$I(\theta_x, \theta_y) = |F(\theta_x, \theta_y)|^2 \frac{\sin^2(M\pi\Lambda_x)\sin(\theta_x/\lambda)\sin^2(N\pi\Lambda_y\sin(\theta_y/\lambda))}{M^2\sin^2(\pi\Lambda_x\sin(\theta_x/\lambda))N^2\sin^2(\pi\Lambda_y\sin(\theta_y/\lambda))}, \tag{11}$$

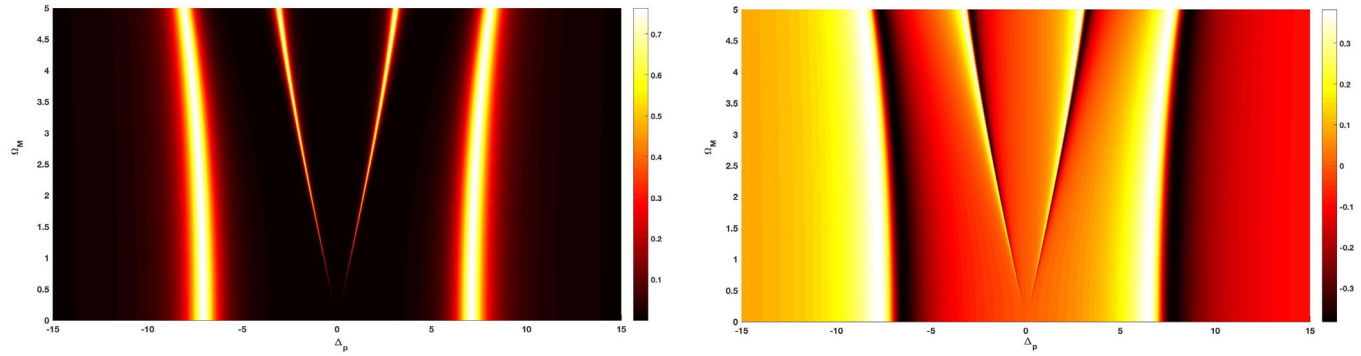

(a) (b)

Fig. 2. (a) Probe absorption and (b) dispersion as a function of Ω_M and Δ_p. The parameters are $\Omega_{c1} = \Omega_{c2} = 5\gamma$, $\Delta_{c1} = \Delta_{c2} = \Delta_M = 0$, $\gamma_{41} = \gamma$, and $\gamma_{51} = \gamma_{31} = \gamma_{21} = 0.1\gamma$.

where λ is the wavelength of the probe field; M and N are the numbers of spatial periods of the atomic grating along the x- and y-axes,

$$F(\theta_x, \theta_y) = \int_0^{\Lambda_x} \int_0^{\Lambda_y} T(x,y) e^{-2i\pi x \sin\theta_x/\lambda} e^{-2i\pi y \sin\theta_y/\lambda} \mathrm{d}x\, \mathrm{d}y \tag{12}$$

is the Fraunhofer diffraction of a single space period; θ_x and θ_y are the diffraction angles along the x- and y-axes.

The (m, n) order of diffraction angle is determined by the grating equations $\sin\theta_x = \frac{m}{x}$ and $\sin\theta_y = \frac{n}{x}$. Therefore, the diffraction intensities of $(0,0)$ order, $(1,0)$ order, $(0,1)$ order and $(1,1)$ order can be obtained as follows:

$$\begin{aligned}
I\left(\theta_x^0, \theta_y^0\right) &= \left| \int_0^{\Lambda_x} \mathrm{d}x \int_0^{\Lambda_y} T(x,y) \mathrm{d}y \right|^2, \\
I\left(\theta_x^1, \theta_y^0\right) &= \left| \int_0^{\Lambda_x} e^{-2\pi i x/\Lambda_x} \mathrm{d}x \int_0^{\Lambda_y} T(x,y) \mathrm{d}y \right|^2, \\
I\left(\theta_x^0, \theta_y^1\right) &= \left| \int_0^{\Lambda_x} \mathrm{d}x \int_0^{\Lambda_y} T(x,y) e^{-2\pi i y/\Lambda_y} \mathrm{d}y \right|^2, \\
I\left(\theta_x^1, \theta_y^1\right) &= \left| \int_0^{\Lambda_x} e^{-2\pi i x/\Lambda_x} \mathrm{d}x \int_0^{\Lambda_y} T(x,y) e^{-2\pi i y/\Lambda_y} \mathrm{d}y \right|^2.
\end{aligned} \tag{13}$$

3 Results and discussion

In this section, the effect of microwave field and other laser field parameters on the diffraction feature of the proposed five-level Rydberg atomic system is investigated. Since the electric susceptibility as the optical response of the probe laser field plays a crucial rule in electromagnetically induced grating. In fig. 2, the absorption and dispersion of the probe field as a function of the probe detuning are plotted. Here, the resonant interaction is considered $\Delta_{c1} = \Delta_{c2} = \Delta_M = 0$.

Figure 2(a) and (b) show the results for imaginary (absorption) and real (dispersion) part of the linear electric susceptibility for the fixed Rabi frequency of coupling Ω_{c1} and Ω_{c2}.

The Rabi frequency of the microwave field and the probe field detuning are varied. There is an EIT window with two side absorption peaks in fig. 2(a), in the absence of microwave field coupling. When the microwave field is applied, two new absorption peaks appear in the EIT window. By increasing the amplitude of the microwave field, the central EIT window becomes wider. Moreover, It is remarkable that the frequency splitting of two central peaks is proportional to the microwave field strength. Accordingly, the magnitude of the applied microwave field can be estimated from their relationship above. Furthermore, the distance between the two side peaks remains unchanged as increase of the microwave field strength.

When the microwave field drives the $|(n+1)P_{3/2}\rangle \leftrightarrow |nD_{5/2}\rangle$ transition, the frequency splitting of two central peaks can be written approximately as

$$\Delta f = 1.4\Omega_M. \tag{14}$$

The corresponding dispersion diagram is shown in fig. 2(b).

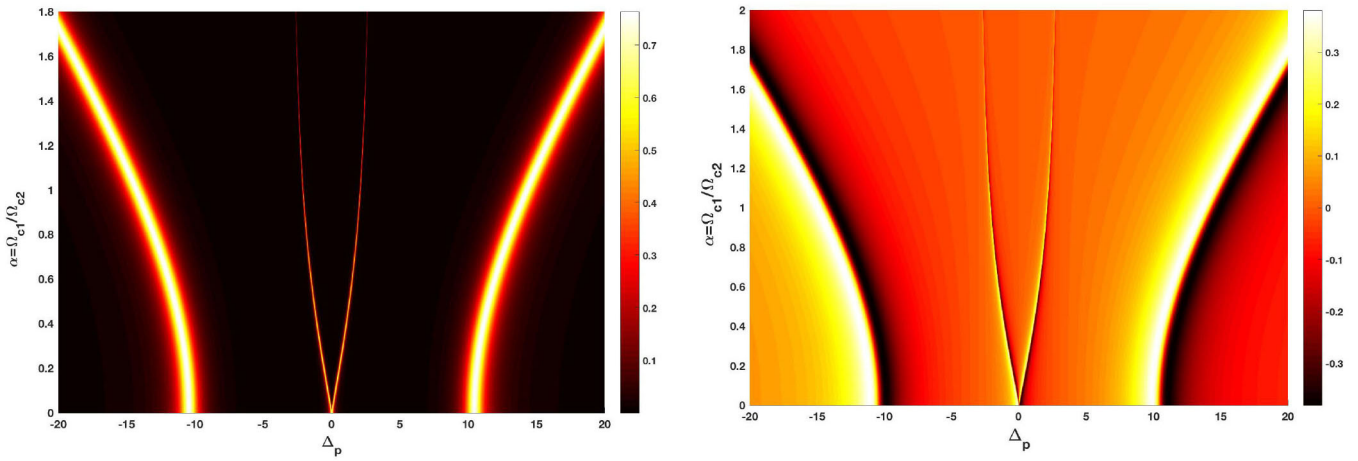

(a) (b)

Fig. 3. (a) Probe absorption and (b) dispersion as a function of $\alpha = \Omega_{c1}/\Omega_{c2}$ and Δ_p. The parameters are $\Omega_M = 3\gamma$, $\Delta_{c1} = \Delta_{c2} = \Delta_M = 0$, $\gamma_{41} = \gamma$, and $\gamma_{51} = \gamma_{31} = \gamma_{21} = 0.1\gamma$.

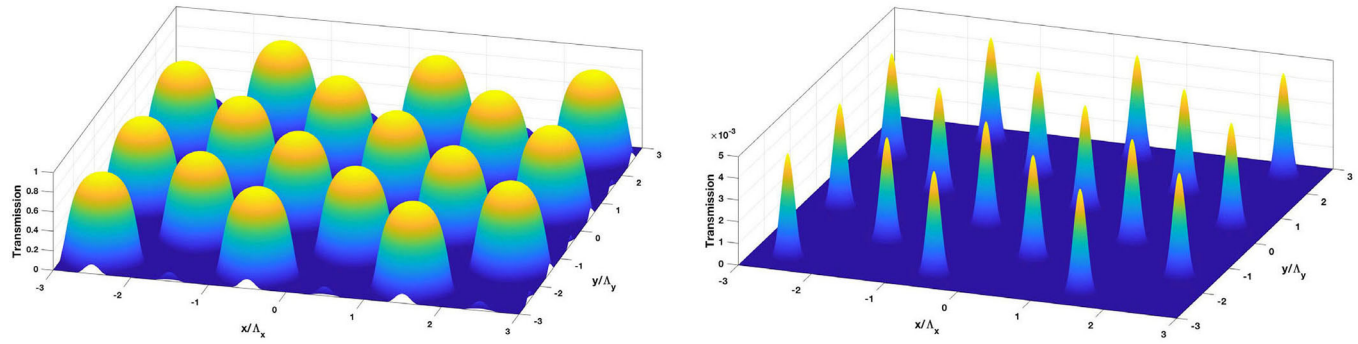

(a) (b)

Fig. 4. The amplitude $T(x, y)$ of the transmission function as a function of x (in units of Λ_x) and y (in units of Λ_y): (a) without microwave field; (b) with microwave field. The parameters are $\Omega_{c1} = \Omega_{c2} = 5\gamma$, $\Omega_M = 3\gamma$, $\Delta_p = 3.093\gamma$, $\Delta_{c1} = \Delta_{c2} = \Delta_M = 0$, $\gamma_{41} = \gamma$, $\gamma_{51} = \gamma_{31} = \gamma_{21} = 0.1\gamma$, and $L = 300\xi$.

The effect of the ratio of two coupling fields Ω_{c1}/Ω_{c2} on the absorption and dispersion is investigated in fig. 3. It can be seen that the position of the two side peaks noticeably is changed in linear absorption spectrums by increasing $\alpha = \Omega_{c1}/\Omega_{c2}$. In addition, it is interesting to find that the frequency splitting of two central peaks gets wider by increasing the ratio of two coupling fields α. When Ω_M is fixed, the change of Δf depends on Ω_{c1}/Ω_{c2}.

It is also noticed that interacting dark resonances much narrow the linewidth of absorption spectrum, which may help to improve the probe accuracy.

It is clear, from fig. 3(a), that the maximum distance is when $\Omega_{c1} = \Omega_{c2}$. Consequently, by increasing α up to more than 1, Δf remains constant. It is enlightening to study the physical mechanism of the above results with the dressed-state theory [24]. Four transition channels exist with the coupling of the probe field corresponding to the left side, two central and right side peaks in fig. 2(a), respectively.

3.1 Absorption grating

The Fraunhofer diffraction intensity of the probe field through a Rydberg atomic system is investigated. The amplitude of the transmission function determines the diffraction pattern here. As was shown in sect. 2, the diffraction intensity depends strongly on the susceptibility of the medium. In all of the calculations and simulations, the three driving fields are considered to be in resonance with their corresponding transitions ($\Delta_{c1} = \Delta_{c2} = \Delta_M = 0$). In order to illustrate the gain modulation, we plot the amplitude $|T(x, y)|$ of the transmission function in fig. 4. In fig. 4, the amplitude $T(x, y)$, depending on the coordinates x and y and microwave field for the weak driving probe field, is plotted. One can see from fig. 4(a) that the probe field, which propagates through the atomic sample, does not lose a significant portion of energy.

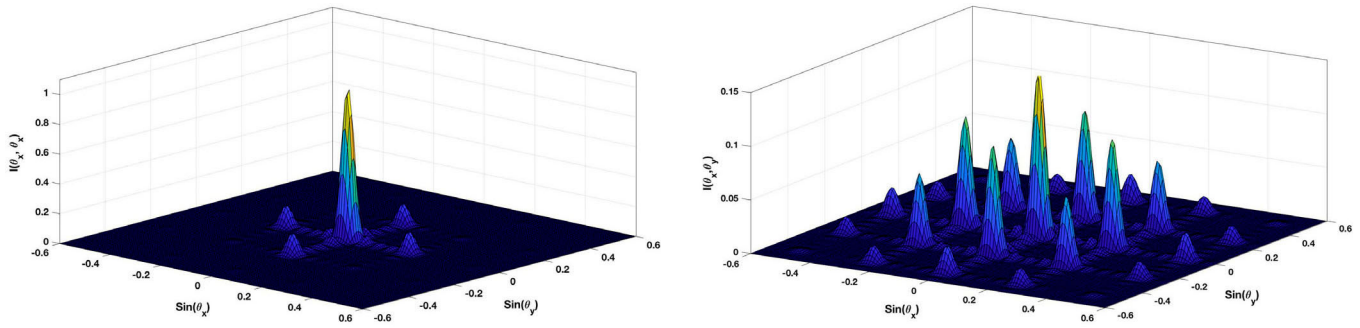

(a) (b)

Fig. 5. The normalized amplitude diffraction intensity $I(\theta_x, \theta_y)$ a function of $\sin(\theta_x)$ and $\sin(\theta_y)$ for the corresponding transmission function shown in fig. 4: (a) without microwave field; (b) with microwave field. The parameters are $\Omega_{c1} = \Omega_{c2} = 5\gamma$, $\Omega_M = 3\gamma$, $\Delta_p = 3.093\gamma$, $\Delta_{c1} = \Delta_{c2} = \Delta_M = 0$, $\gamma_{41} = \gamma$, $\gamma_{51} = \gamma_{31} = \gamma_{21} = 0.01\gamma$, $M = N = 5$, and $L = 300\xi$.

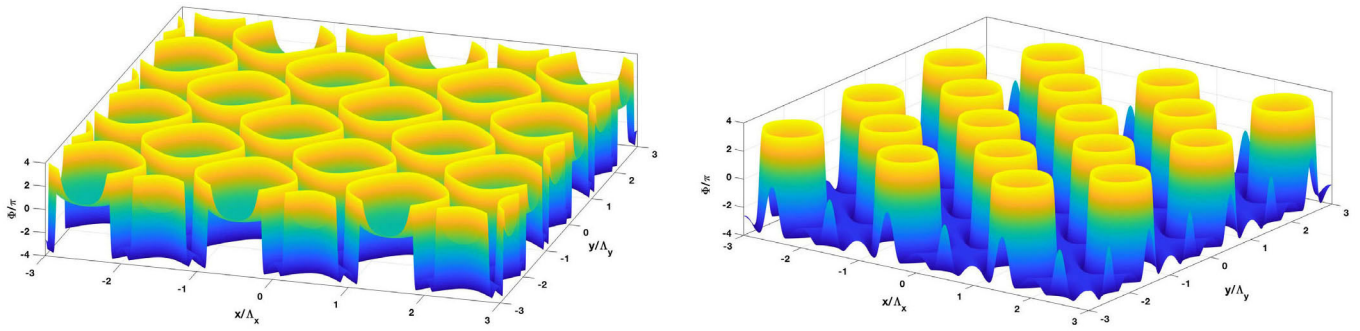

(a) (b)

Fig. 6. The phase $\Phi(x, y)/\pi$ of the transmission function as a function of x (in units of Λ_x) and y (in units of Λ_y): (a) without microwave field; (b) with microwave field. The parameters are $\Omega_{c1} = \Omega_{c2} = 5\gamma$, $\Omega_M = 3\gamma$, $\Delta_p = 3.093\gamma$, $\Delta_{c1} = \Delta_{c2} = \Delta_M = 0$, $\gamma_{41} = \gamma$, $\gamma_{51} = \gamma_{31} = \gamma_{21} = 0.1\gamma$, and $L = 300\xi$.

As is shown in fig. 4(b), it is clear that the space-dependent amplitude suppression happens in the system in the presence of microwave field. Consequently, an absorption grating is formed in the medium. Similar to one-dimensional gain grating, the gain modulation plays a fundamental role in enhancing the diffraction efficiency. So as to show the 2D diffraction based on the spatially modulated gain of the probe field in the present system, the Fraunhofer diffraction intensity $I(\theta_x, \theta_y)$ is plotted in fig. 5 as a function of $\sin(\theta_x)$ and $\sin(\theta_y)$ for investigating the effect of microwave field on electromagnetic induced amplitude grating. At the absence of applied microwave field, probe light does not diffract to higher orders of grating and from fig. 5(a), $I(\theta_x^1, \theta_y^0)$ and $I(\theta_x^0, \theta_y^1)$ are just appeared, while, in the presence of microwave field, higher orders of diffraction, such as $I(\theta_x^1, \theta_y^1)$, $I(\theta_x^2, \theta_y^0)$ and $I(\theta_x^0, \theta_y^2)$ show higher efficiency. Moreover, the efficiency of $I(\theta_x^1, \theta_y^0)$ and $I(\theta_x^0, \theta_y^1)$ increased considerably. These results are based on gain modulation accompanied by microwave field, which could help enhance the diffraction efficiency in high-order directions. At the same time, the central light intensity would become weak and most of the probe light is diffracted. Definitely, the diffraction intensities could be greatly enhanced via increasing the amplitude of coupling fields, the atoms or the interaction length. It is discovered that the first-order diffraction intensity can reach to its maximal value under an appropriate Ω_M. In fig. 5(b), the energy transfers from the center maximum to high-order diffraction peaks.

3.2 Phase grating

The phase of the transmission function determines the diffraction pattern here. As is shown in fig. 6, $\Phi(x, y)$ of the probe field changes periodically in the x- and y-directions, which deflects the probe beam intensity out of the zeroth diffraction into additional side diffraction patterns.

As pointed out in the above discussion, the diffraction efficiency via absorption grating is very small and limited due to the large absorption. Therefore, the probe energy can be diffracted from zeroth-order into high-order directions due to the large phase modulation. By applying the microwave field, it is obvious, from fig. 7(b), that the phase modulation becomes dominant and the diffracting power increases notably.

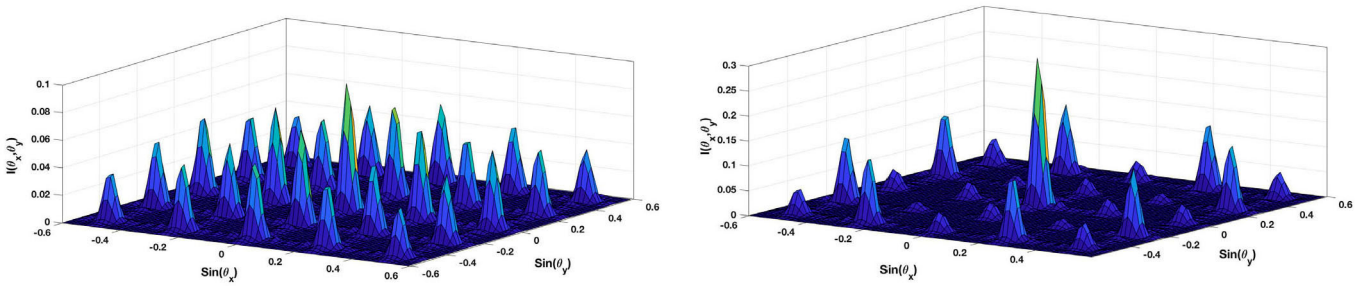

(a) (b)

Fig. 7. The normalized phase diffraction intensity $I(\theta_x, \theta_y)$ a function of $\sin(\theta_x)$ and $\sin(\theta_y)$ for the corresponding transmission function shown in fig. 6: (a) without microwave field; (b) with microwave field. The parameters are $\Omega_{c1} = \Omega_{c2} = 5\gamma$, $\Omega_M = 3\gamma$, $\Delta_p = 3.093\gamma$, $\Delta_{c1} = \Delta_{c2} = \Delta_M = 0$, $\gamma_{41} = \gamma$, $\gamma_{51} = \gamma_{31} = \gamma_{21} = 0.1\gamma$, $M = N = 5$, and $L = 300\xi$.

In such a circumstance, the atomic system reaches a reasonable level of transparency across the probe beam with enhanced refraction due to the destructive quantum interference of microwave field, hence a large phase modulation on the probe field to higher orders $I(\theta_x^1, \theta_y^2)$ and $I(\theta_x^2, \theta_y^1)$ can be initiated.

4 Conclusion

In conclusion, 2D electromagnetically induced grating in a five-level Rydberg atomic system driven by two standing-wave fields is investigated. A double-dark-state system is used to improve sensitivity of 2D EIG to microwave field. Interacting dark resonances boost the linear absorption and two central peaks which are very delicate to the Rabi frequency of the microwave field. Increasing the ratio of two coupling field strengths enhances the higher probe sensitivity. Consequently; a sensitive 2D EIG can be observed. The numerical calculations show that the high orders of 2D phase and amplitude EIG can be improved via microwave field compared to the single-dark-state system. This proposed system would be suitable for designing novel microwave sensing devices in optical networking and communication.

References

1. L. Deng, M.G. Payne, W.R. Garrett, Phys. Rev. A **64**, 023807 (2001).
2. L.V. Hau, S.E. Harris, Z. Dutton, C.H. Behroozi, Nature **397**, 594 (1999).
3. T. Naseri, S.H. Asadpour, R. Sadighi-Bonabi, J. Opt. Soc. Am. B **30**, 641 (2013).
4. Y. Wu, J. Saldana, Y. Zhu, Phys. Rev. A **67**, 013811 (2003).
5. J.W.R. Tabosa, A. Lezama, G.C. Cardoso, Opt. Commun. **165**, 59 (1999).
6. G.C. Cardoso, J.W.R. Tabosa, Phys. Rev. A **65**, 033803 (2002).
7. J. Sheng, J. Wang, M.-A. Miri, D.N. Christodoulides, M. Xiao, Opt. Express **23**, 19777 (2015).
8. L. Zhao, Sci. Rep. **8**, 3073 (2018).
9. R. Sadighi-Bonabi, T. Naseri, M. Navadeh-Toupchi, Appl. Opt. **54**, 368 (2015).
10. T. Naseri, R. Sadighi-Bonabi, J. Opt. Soc. Am. B **31**, 2430 (2014).
11. F. Zhou, Y. Qi, H. Sun, D. Chen, J. Yang, Y. Niu, Sh. Gong, Opt. Express **21**, 12249 (2013).
12. Sh. Kuang, Ch. Jin, Ch. Li, Phys. Rev. A **84**, 033831 (2011).
13. T. Naseri, R. Moradi, Superlattices Microstruct. **101**, 592 (2017).
14. S.A. Ziauddin, Sh. Qamar, S. Qamar, Phys. Rev. A **94**, 033823 (2016).
15. F. Bozorgzadeh, M. Sahrai, Phys. Rev. A **98**, 043822 (2018).
16. J. Lim, H-g. Lee, J. Ahn, J. Kor. Phys. Soc. **63**, 867 (2013).
17. H. Fan, S. Kumar, J. Sedlacek, H. Kubler, S. Karimkashi, J.P. Shaffer, J. Phys. B **48**, 202001 (2015).
18. J.A. Sedlacek, A. Schwettmann, H. Kubler, R. Low, T. Pfau, J.P. Shaffer, Nat. Phys. **8**, 819 (2012).
19. G.-L. Cheng, L. Cong, A.-X. Chen, J. Phys. B **49**, 085501 (2016).
20. J.-Ch. Wu, T.-T. Hu, Laser Phys. Lett. **15**, 065202 (2018).
21. L. Wang, F. Zhou, P. Hu, Y. Niu, Sh. Gong, J. Phys. B **47**, 225501 (2014).
22. T. Qiu, G. Yang, J. Phys. B **48**, 115504 (2015).
23. H.Y. Ling, Y.-Q. Li, M. Xiao, Phys. Rev. A **57**, 1338 (1998).
24. L. Zhang, Y. Jiang, R. Wan, S. Tian, B. Shang, X. Zhang, J. Gao, Y. Niu, S. Gong, J. Phys. B **44**, 135505 (2011).